

DESY SR-84-06

March 1984

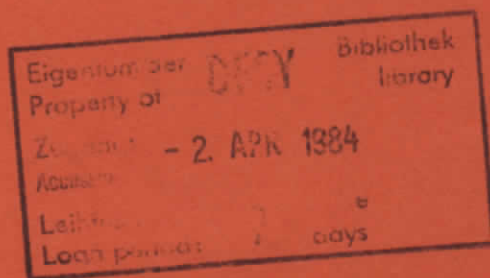
X-RAY STANDING WAVE MODULATED ELECTRON EMISSION NEAR ABSORPTION
EDGES IN CENTRO - AND NONCENTROSYMMETRIC CRYSTALS

by

M.J. Bedzyk, G. Materlik

Hamburger Synchrotronstrahlungslabor HASYLAB at DESY

M.V. Kovalchuk

Inst. of Crystallography, Acad.Sci. of the USSR, Moscow

ISSN 0723-7979

NOTKESTRASSE 85 · 2 HAMBURG 52

DESY behält sich alle Rechte für den Fall der Schutzrechtserteilung und für die wirtschaftliche Verwertung der in diesem Bericht enthaltenen Informationen vor.

DESY reserves all rights for commercial use of information included in this report, especially in case of filing application for or grant of patents.

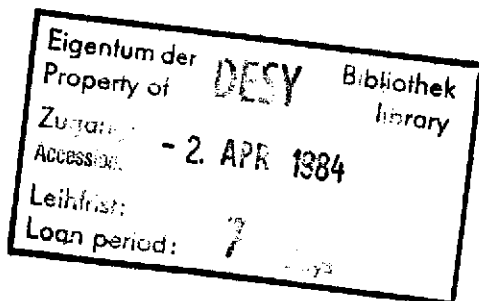
To be sure that your preprints are promptly included in the
HIGH ENERGY PHYSICS INDEX ,
send them to the following address (if possible by air mail) :

DESY
Bibliothek
Notkestrasse 85
2 Hamburg 52
Germany

X-ray Standing Wave Modulated Electron Emission
near Absorption Edges
in Centro - and Noncentrosymmetric Crystals

M.J. Bedzyk and G. Materlik
Hamburger Synchrotronstrahlungslabor HASYLAB at
Deutsches Elektronen-Synchrotron DESY
D-2000 Hamburg 52, Germany

M.V. Kovalchuk
Institute of Crystallography
Academy of Sciences of the USSR
Moscow 117333, USSR



Abstract

Energy dispersive electron emission yields were measured for (111) Bragg reflections of x-rays from perfect Ge and GaAs crystals. The reflection angle was changed continuously over the Bragg reflection range, thus causing the internal x-ray standing wave pattern to move across the atomic planes. Using synchrotron radiation, these measurements were performed at photon energies below and above the Ga and As K absorption edges. This introduces an energy dependent position shift of the noncentrosymmetric diffraction planes relative to the atomic planes. It is shown how to determine from such measurements: (i) the dispersion parameters f' and f'' , (ii) lattice deviations, including amorphous and crystalline surface layers, (iii) a mean electron escape depth, and (iv) crystal polarity.

PACS numbers: 61.60.+m; 61.10.Fr; 61.80-x; 68.20+t

I. Introduction

The interpretation of phenomena, which occur in perfect crystals under the condition of dynamical X-ray diffraction, in terms of X-ray standing waves, is a well established procedure since the discovery of the Borrmann effect¹. This picture, which relates the X-ray standing wave field structure to the crystal structure, was at first applied to explain the anomalous transmission of incident X-rays. Batterman² was thereafter, the first to study a related emission process, namely the case of K fluorescence from a Ge crystal while Bragg reflecting incident Mo K α radiation. Other basic processes involved in X-ray scattering such as: thermal diffuse scattering^{3,4}, Compton scattering^{3,5,6}, and electron emission^{7,8}, were also investigated in first experiments during the following years.

In 1974, the possibility to use the movement of X-ray standing waves to determine the position of impurity atoms in a host lattice was demonstrated by Golovchenko, Batterman and Brown⁹ by using characteristic fluorescence radiation. Later, this technique was also applied to locate chemisorbed atomic layers on crystal surfaces^{10,11}.

Independently developed, was a method to use electron emission for studying distortion profiles of disturbed surface layers⁷ and of epitaxially grown surface layers with varying thicknesses¹².

Previous to our investigation, X-ray standing wave measurements on noncentrosymmetric crystals have been used to determine

the polarity of GaP crystals orientated in the (111) direction. The first such investigation, made by Trucano¹³, monitored the K-fluorescence from the phosphorus atomic planes as the nodal planes of the standing wave field moved across the phosphorus atomic planes when sweeping through the (111) Bragg reflection and across the Ga atomic planes for the ($\bar{1}\bar{1}\bar{1}$) case.

Subsequently, Takahashi and Kikuta⁸, performing a similar investigation, monitored the zero energy loss Ga L-photoelectrons, using a cylindrical energy analyser in a high vacuum chamber.

Unlike the absorption length of the reemitted fluorescence radiation, the photoelectron escape depth is very small in comparison to the extinction length of the incident X-rays. This feature plus the depth dependent electron energy loss process give the photoelectron standing wave measurement certain distinctive structural determining advantages in comparison to the fluorescence measurement. Since high energy resolution photoelectron measurements present certain technical difficulties, namely the need for high vacuum and longer data collection time, it can be advantageous to use a low resolution electron counter. Parallel to our investigation, Patel and Golovchenko¹⁴, in a standing wave measurement on GaAs(111), have collected the fluorescence with a glancing angle detector geometry. Thus they were able to reduce the extinction dip feature which masks structural information when the absorption length of the emitted characteristic radiation becomes comparable with the extinction depth of the incident radiation.

In this paper we report measurements made with noncentrosymmetric GaAs crystals along with comparative results from centrosymmetric Ge crystals, and show how a proportional counter can be used as an electron spectrometer in combination with synchrotron radiation. The energy tunability of the incident photons makes

it possible to take measurements below and above the absorption edges of the atomic species which constitute the crystal. Thus, the experiment demonstrates how to measure the shift of the noncentrosymmetric diffraction planes with respect to the atomic lattice as a function of photon energy. This position shift is based on the fact that X-ray diffraction is connected with the Fourier component of the elastically scattering charge density described by the structure factor of the reflection which changes strongly close to absorption edges. The dispersion parameters f' and f'' are used to characterize the energy dependence of this process. Therefore, these can also be determined from such measurements.

At a fixed incident photon energy, one can obtain structural information on different levels of spatial sensitivity by monitoring the electron emission at different angular points in the vicinity of the strong Bragg reflection. Electrons, which are inelastically scattered on their way out of the crystal, have a specific energy loss which is related to the depth at which the initial photon absorption and electron reemission took place. This leads to structural information in units of the electron mean free path. Atomic positions on the scale of the diffraction plane spacing can be determined by measuring the angular variation of the electron emission from a particular atomic species.

II. Theory

In this section, information pertaining to the dynamical theory of noncentrosymmetric diffraction from a GaAs(111) perfect

crystal will be given. The specialization of the analysis for centrosymmetric structures will be straightforward. For a general review of the dynamical theory of X-ray diffraction see Refs. 15 and 16, and for applications of this theory to zinc blend single crystals see Refs. 13 and 8.

For the two beam plane wave case of Bragg diffraction from a semi-infinitely thick and symmetrically cut crystal (i.e. the diffraction planes are parallel to the surface), the ratio of the E-field amplitudes can be written as:

$$\frac{E_H}{E_0} = - \frac{|P| \sqrt{\frac{F_H}{F_H^*}}}{P} [\eta \pm (\eta^2 - 1)^{1/2}], \quad (1)$$

where the dimensionless angular parameter η is:

$$\eta = \frac{-\Delta\theta \sin 2\theta_B + \Gamma F_0}{|P| \Gamma (F_H F_H^*)^{1/2}} \quad (2)$$

In this notation¹⁵, $\Delta\theta = \theta - \theta_B$, $\Gamma = (r_e \lambda^2)/(\eta V)$, $P = 1$ for σ polarization and $P = \cos 2\theta_B$ for π polarization. F_H and F_H^* are the structure factors for the respective (h, k, l) and $(-h, -k, -l)$ planes in reciprocal space. r_e is the classical electron radius, λ the incident photon wavelength and V the volume of the unit cell.

The structure factor is described in terms of the arrangement of the "N" atoms within the unit cell as:

$$F_H = \sum_{n=1}^N (f_H^0 + f_H' + i f_H'')_n e^{2\pi i \underline{H} \cdot \underline{r}_n} \quad (3)$$

The atomic form factor $f_{H,n}^0$ accounts for the coherent scattering of X-rays from electrons within the electron distribution of the n^{th} atom. It is energy independent and depends on the mag-

nitude of the scattering vector $\sin\theta/\lambda$. However, if inelastic photon scattering processes are included, the initial and final quantum states affect the phase of a scattered photon. This is usually described by adding a real $f_{H,n}^i$ and an imaginary $f_{H,n}^{i'}$ anomalous dispersion correction to $f_{H,n}^0$.

Position vector \underline{r}_n locates the center of the n^{th} atom with respect to an arbitrarily chosen reference system. For the case of GaAs we will choose a reference system in which the four Ga atoms in the unit cell have positions $(0,0,0) + fcc$ and the four As atoms have positions $(1/4,1/4,1/4) + fcc$.

The resulting structure factor will be complex having the form:

$$F_H = F_H^i + iF_H^{i'} \quad (4)$$

with the real quantities F_H^i and $F_H^{i'}$ being:

$$F_H^i = \begin{cases} 4(f_{Ga}^0 + f_{Ga}^i + f_{As}^{i'})_H & \text{for } h, k, \ell \text{ all odd and } \frac{h+k+\ell+1}{4} \\ & \text{an integer,} \\ 4(f_{Ga}^0 + f_{Ga}^i - f_{As}^{i'})_H & \text{for } h, k, \ell \text{ all odd and } \frac{h+k+\ell+1}{4} \\ & \text{not an integer} \\ 4(f_{Ga}^0 + f_{Ga}^i + f_{As}^0 + f_{As}^{i'})_H & \text{for } h, k, \ell \text{ all even and } \frac{|h|+|k|+|\ell|}{4} \\ & \text{an integer} \\ 4(f_{Ga}^i - f_{As}^i + f_{Ga}^0 - f_{As}^0)_H & \text{for } h, k, \ell \text{ all even and } \frac{|h|+|k|+|\ell|}{4} \\ & \text{not an integer,} \\ 0 & \text{otherwise,} \end{cases} \quad (5a)$$

and

$$F_H^{i'} = \begin{cases} -4(f_{As}^0 + f_{As}^{i'} - f_{Ga}^{i'})_H & \text{for } h, k, \ell \text{ all odd and } \frac{h+k+\ell+1}{4} \\ & \text{an integer,} \\ 4(f_{As}^0 + f_{As}^{i'} + f_{Ga}^{i'})_H & \text{for } h, k, \ell \text{ all odd and } \frac{h+k+\ell+1}{4} \\ & \text{not an integer} \\ 4(f_{Ga}^{i'} + f_{As}^{i'})_H & \text{for } h, k, \ell \text{ all even and } \frac{|h|+|k|+|\ell|}{4} \\ & \text{an integer,} \\ 4(f_{Ga}^{i'} - f_{As}^{i'})_H & \text{for } h, k, \ell \text{ all even and } \frac{|h|+|k|+|\ell|}{4} \\ & \text{not an integer,} \\ 0 & \text{otherwise.} \end{cases} \quad (5b)$$

The "h, k, ℓ all odd" cases of Eq. (5) correspond to noncentrosymmetric planes, which means $F_H \neq F_{\bar{H}}$. The "h, k, ℓ all even with $[|h|+|k|+|\ell|]/4$ not an integer" case corresponds to a semi-forbidden reflection in which the Ga lattice and As lattice do not completely produce destructive interference.

Compensation for thermal vibrations can be made by multiplying the structure factor by the appropriate Debye-Waller factor e^{-M} . For GaAs(111) we shall approximate the vibrational amplitude of the Ga and As atoms as being equivalent ($e^{-M_{Ga}} = e^{-M_{As}} = 0.979$, at $T=293^\circ$ K, Ref. 17). The reflectivity is:

$$R = \left| \frac{E_H}{E_0} \right|^2. \quad (6)$$

Figure 1 shows calculated GaAs(111) reflectivity curves for X-ray energies close to the Ga ($E_k = 10.367$ keV) and As ($E_k = 11.863$ keV) K-absorption edges. As can be seen, the shape is strongly influenced by the inelastic absorption process. The E-field intensity at a position \underline{r} in the crystal is proportional to

$$I = e^{-\mu_z z^2} \left[1 + \left| \frac{E_H}{E_0} \right|^2 + 2P \left| \frac{E_H}{E_0} \right| \cos(v + 2\pi \underline{H} \cdot \underline{r}) \right], \quad (7)$$

where

$$v = \tan^{-1} \left[\frac{\text{Im}(E_H/E_0)}{\text{Re}(E_H/E_0)} \right]. \quad (8)$$

The phase angle v changes in a continuous fashion by π radians as the crystal is rotated through the strong Bragg diffraction condition. In terms of $\eta' = \text{Re}(\eta)$, it can be seen from Eq.

(1) that the strong Bragg diffraction region corresponds to $|\eta'| < 1$.

The effective linear absorption coefficient μ_z , which is used in Eq. (7) can be expressed as:

$$\mu_z = \frac{\mu_0}{\sin \theta_B} \left[1 + \frac{P}{F_0'} \text{Im} \left(F_H \frac{E_H}{E_0} \right) \right], \quad (9)$$

where the normal linear absorption coefficient is:

$$\mu_0 = (2\pi/\lambda) \Gamma F_0' = (8\pi/\lambda) \Gamma (f_{Ga}' + f_{As}'). \quad (10)$$

For depths much smaller than the extinction depth, i.e., $z \ll \lambda \sin \theta_B / (2\pi \Gamma) / (|F_0'| + \sqrt{|F_H| |F_H'|})$, the exponential attenuation term in Eq. (7) can be neglected. For 15 keV X-rays diffracted from GaAs(111) this corresponds to $z \ll 0.3 \mu\text{m}$. Thus the E-field intensity near the surface is proportional to:

$$I = 1 + \left| \frac{E_H}{E_0} \right|^2 + 2P \left| \frac{E_H}{E_0} \right| \cos(v - 2\pi \frac{\Delta d}{d}), \quad (11)$$

where $d = 1/|H|$ is the d-spacing and Δd measures the displacement in the \underline{H} direction from our arbitrarily chosen origin to position \underline{r} . Eq. (11) indicates that during Bragg diffraction a standing wave field is produced, which has the same periodicity as the diffraction planes. Furthermore, as the angle of incidence is advanced through the strong Bragg reflection the phase angle v changes in a linear fashion by π radians, thus causing the antinodes of the standing wave field to move inward by one half of a d-spacing.

In order to find the position of the noncentrosymmetric diffraction planes in this reference system, one applies the condition to Eq. (11) that the antinodal planes of the E-field intensity coincide positionally with the diffraction planes for $\eta' \leq -1$. This corresponds to the high angle side of the strong Bragg reflection.

From Eq. (11), the maximum in the E-field intensity occurs at a position Δd_0 when

$$\frac{\Delta d_0}{d} = \frac{v}{2\pi}. \quad (12)$$

Using $\eta = -1$ in Eq. (1) and the resulting expression in Eq. (8) results in:

$$\frac{\Delta d_0}{d} = \frac{1}{4\pi} \left[\tan^{-1} \left(\frac{F_H'}{F_H} \right) - \tan^{-1} \left(\frac{F_H^{1'}}{F_H} \right) \right]. \quad (13)$$

The expressions in Eq. (5) can be used for describing the centrosymmetric diamond structure case of Ge(111) by replacing both Ga and As with Ge. From this operation the resulting $\Delta d_0/d = -1/8$.

This corresponds to the centrosymmetric diffraction plane position, which is located halfway between the Ga and As layers, as seen in Fig. 2. For the noncentrosymmetric case of GaAs (111), the diffraction planes are shifted from this centrosymmetric position by an amount Δ_{111} . From Eq. (13) this non-centrosymmetric shift is determined as:

$$\Delta_{111} = -\frac{1}{8+4\pi} \left[\tan^{-1} \left(\frac{f_{As}^0 + f_{As}' + f_{Ga}'''}{f_{Ga}^0 + f_{Ga}' - f_{As}'''} \right) + \tan^{-1} \left(\frac{f_{As}^0 + f_{As}' - f_{Ga}'''}{f_{Ga}^0 + f_{Ga}' + f_{As}'''} \right) \right]. \quad (14)$$

Since the dispersion corrections are energy dependent the position of the diffraction planes with respect to the atomic planes is also energy dependent.

Hence, for noncentrosymmetric Bragg reflection the diffraction planes have an energy adjustable phase with respect to the atomic lattice. This shift due to dispersion is most evident in GaAs(111) when comparing the E-field intensities at the Ga and As atomic sites for X-ray energies at the respective absorption edges. In Fig. 3, the theoretical E-field intensities at the Ga and As atomic sites in GaAs(111) are shown for $E_\gamma = 10.372$ keV (5 eV above Ga K-edge) and $E_\gamma = 11.868$ keV (5 eV above As K-edge). At $E_\gamma = 10.372$ keV, $\Delta_{111} = 0.016$ and at $E_\gamma = 11.868$ keV, $\Delta_{111} = -0.015$ (see Table 1). Although the resulting shift only corresponds to 0.031 of a d_{111} spacing the change in the E-field intensity is appreciable as can be seen in Fig. 3. Since the photoelectric absorption of an atom is proportional to the E-field intensity at the site of the atom it becomes possible to determine the energy dependent position of the diffraction planes by analysing the yield of the Ga or As photoelectrons during Bragg diffraction.

III. Experiment

The measurements were carried out with synchrotron radiation generated by the storage ring DORIS at DESY in Hamburg. The instrument ROEMO at the Hamburger Synchrotron Radiation Laboratory HASYLAB provided the basic experimental features for standing wave measurements²¹. The arrangement is illustrated in Fig. 4. The polarized white spectrum of DORIS gives high angular brightness and photon energies optimized for the absorption edges being studied. A narrow energy band is selected by a double crystal monochromator using Si(111) single crystals in a parallel mode. The second crystal is asymmetrically cut, having an angle of $\psi = 7^\circ$ between the surface and the (111) Bragg planes, thus serving as a plane wave generator, with a total angular emittance range of 0.67 arc sec at 15.1 keV. This width is small compared to that of the GaAs(111) reflection from the sample (8.3 arc sec). Since the respective (111) d-spacings for the Si, GaAs and Ge lattice planes differ only slightly, the dispersion of the arrangement is normally small enough for standing wave applications. Ge(111) data, which we have measured, are not discussed in detail to limit the total length of this paper.

The sample is built into a gas flow proportional detector^{22,23}. Photoelectrons and Auger electrons, emitted from the sample, ionize the gas volume, which consists of a 90 % Helium + 10 % methane mixture. After gas multiplication, the resulting cascade is collected at a 20 μm thin gold wire. The efficiency of the chosen gas mixture is very high for ionization by electrons

with a kinetic energy in the keV range and very small ($< 1\%$) for the incident and reflected synchrotron X-radiation. The output signal from the wire is pulse height analysed, after pre- and main amplification, in an analog to digital converter, which is connected to a multi-channel analyser (MCA). The MCA is operated in a multi spectrum scaling mode, which means that up to 32 subgroups are collected with different electron yield spectra. Each subgroup is directly related to a small angular fraction of the sample reflection curve²¹. The resolution of the detector is about 1 keV for the electron energies used.

The whole detector was mounted on an Eulerian cradle with a special stage for standing wave experiments²⁴. The reflected intensity was monitored with a NaI (Tl) detector.

In this experimental arrangement, the horizontal polarization direction of the synchrotron radiation is perpendicular to both the incident and diffracted wave vectors. This corresponds to the σ polarization state.

The total electron yield from the sample was approximately 5×10^{-4} electrons per photon, at an incident photon energy of 15 keV. Since the primary beam contains about 10^8 phot./mm², small sample areas are sufficient to provide enough signal to perform standing wave analysis. Therefore, with a two dimensional collimator, the proper region of the crystal can be chosen and three dimensional information can be extracted about crystal defects, epitaxially grown layers or amorphous surface layers²⁵). Planar information is reached by scanning and the depth profile is connected with the electron energy loss process which is described in the following sections.

The absorption of photons is followed by the emission of photoelectrons, fluorescence radiation and Auger electrons. Reemitted photons have so far been successfully used to study the local position of implanted atoms and surface layers. Characteristic for this process is the narrow, well defined photon line shape with a width of some eV. Usually, the detector resolution (typically 160 eV) by far outweighs this inherent line width.

Electrons, emitted at a depth inside the crystal, however, have only a very short mean free path before they undergo an inelastic electron-electron or electron-plasmon interaction. If they are created in the crystal with an initial kinetic energy, they reach the surface and finally the detector with an energy loss, which depends upon their origin and upon the sample material. When they originate from layers close to the surface, this loss can be zero. In high resolution X-ray photoelectron spectroscopy a zero-loss line²⁶ appears.

Electron yield spectra which were recorded with the previously described detector at different photon energies incident on a (111) GaAs single crystal are shown in Fig. 5. Also shown in Fig. 5 is an absorption spectrum. The absorption spectrum was measured by using the total electron yield signal, which is proportional to the number of photons being absorbed in the sample.

Curve 5a) at the bottom of Fig. 5 was measured for a photon energy just below the Ga K absorption edge. The broad photoelectron peak mainly consists of L photoelectrons which have a maximum energy of $E_{kin,max} = E_{\gamma} - E_{L_3} = 8.95$ keV, where E_{γ}

and E_{L_3} correspond to the photon energy and to the L_3 Ga electron binding energy, respectively. Also contributing are electrons from other Ga L subshells as well as from As L states. The yield at energies closer to E_Y is effected by transitions from outer M and valence states. However, the cross section for photoabsorption of these outer electron states is much smaller. This can be seen for the respective cross sections of Ga. At 9.88 keV, which corresponds to the Ge K_{α} line, $\sigma_L = 3190$ barns/atom, $\sigma_M = 471$ barns/atom and $\sigma_N = 15.2$ barns/atom (from Ref. 27).

At an energy 5 eV above the Ga K absorption edge (Fig. 5b), K photoelectron emission as well as K XY Auger electron emission are turned on. For the case of K L_2 L_3 these Auger electrons are clearly visible in the increased yield below the energy $E_{kin,Auger} = 8.04$ keV. K photoelectrons are not detected because their kinetic energy is too small (< 5 eV).

As one increases the energy to above the As K absorption edge, K XY Auger electrons from As atoms are also emitted (Fig. 5d). The Ga K photoelectrons now also have enough kinetic energy so that they appear in the peak at about 500 eV. When the energy is raised further to 15.1 keV (Fig. 5e) both Ga and As K photoelectron peaks are clearly distinguishable.

The energy scale which is given for these spectra has been determined by comparing the same electron process at different photon energies. The Auger electron yield for example can be extracted by subtracting the spectrum below an absorption edge from that above the edge.

As described in Sec. II, the standing wave pattern created inside the sample crystal under the condition of Bragg reflection

can be moved across the netplanes by changing the reflection angle. Electron yield spectra which were measured with a fixed photon energy at several angles within and just outside the total reflection range are shown in Fig. 6. Note, that the As K photoelectron peak (region A) is strongly depressed at angle position 20. Referring to Fig. 2 this corresponds to a node in the wavefield being located at $\phi = -0.125 + \Delta$, right on the As atom sites. At angle position 10, the high angle side of the reflection range (see Fig. 7), the maxima of the standing wave pattern lie on the diffraction planes $\phi = 0$. This behaviour demonstrates the ability of this method to determine the polarity of the crystal by one single measurement. Reflecting at $(\bar{1}\bar{1}\bar{1})$ planes exchanges the Ga and As atomic planes in Fig. 2.

V. Data Analysis and Results

A primary objective of an X-ray standing wave analysis is to determine the atomic distribution function of a particular set of atoms. This is usually characterized by the coherent fraction f_c of atoms occupying coherent positions ϕ_c in units of the diffraction plane spacing d_{hkl} . When using a detector system with sufficient energy resolution it is possible to identify ϕ_c and f_c with a specific set of atoms (Ga or As) undergoing selective excitation of a particular electron state. For the ~ 1 keV resolution of our electron counter and a sample with two almost adjacent elements, the measured electron yield contains in each electron energy region of the spectrum, contributions from both Ga and As. However, f_c and ϕ_c still contain useful structural information which will be demonstrated in this analysis by combining measurements at different photon energies.

The coherent position and fraction for a particular electron energy region is determined by fitting the experimental angular yield for this region to angular E-field intensity expressions based on dynamical diffraction theory.

For the experimental angular yield, the total counts in each region were normalized for dead time effects and then given a pulse pile-up correction. The lifetime for each spectrum was determined from the random reference pulser signal. The pulse pile-up correction was determined by an experimental simulation.

The theoretical model that was given a χ^2 fit to the experimental angular yield data has the following form:

$$Y(\theta, \phi_c, f_c, z) = f_c I(\theta, \phi_c, z) + (1-f_c) [1+R(\theta)] e^{-\mu_z z} \quad (15)$$

The E-field intensity $I(\theta, \phi_c, z)$ is given in Eq. (7), R is the reflectivity (see Eq. (6)), and μ_z is the effective absorption coefficient described by Eq. (9). The first term in Eq. (15) corresponds to the angular yield from a coherent fraction f_c of atoms, which have the periodicity of the diffraction planes and are at a coherent position ϕ_c with respect to the diffraction planes (see Fig. 2 for an explanation of the ϕ scale). The second term describes the remaining fraction of atoms as being randomly distributed. The $e^{-\mu_z z}$ factor in both terms accounts for the angular dependent attenuation of the X-ray wave field (extinction effect). In our analysis we approximate that all of the electrons in a given electron energy region originate from the same depth z . This depth z was not a variable parameter for the GaAs(111) data analysis, but was predetermined

from Ge(111) data. This was a necessary procedure since the parameters z and ϕ_c do not correlate well in the fitting process. For the Ge(111) data analysis the coherent position was naturally fixed at $\phi_c = 0$. Including the $e^{-\mu_z z}$ attenuation factor, significantly improved the χ^2 fits of Eq. (15) to the experimental angular yield data.

Though the detailed electron scattering process causes a complicated profile for electrons escaping from the solid with a particular energy loss, the above delta function approximation for this profile is sufficient for the analysis, provided that the electron escape depth is smaller than the x-ray extinction depth.

The validity of modelling the distribution of atoms as a coherent fraction f_c at a position ϕ_c and the remaining fraction of atoms being randomly distributed, stems from the fact that the X-ray standing wave measurement determines the (hkl) Fourier component of the distribution function of inelastic scatterers.

For a particular electron energy region the distribution function of Ga and As atoms with a (111) d-spacing periodicity can be written as:

$$g(\phi) = G \delta(\phi - \frac{1}{8} \Delta) + (1-G) \delta(\phi + \frac{1}{8} \Delta) \quad , \quad (16)$$

where G represents the fractional yield of the electron energy region which originated from Ga atoms at position $\phi = \frac{1}{8} \Delta$ (see Fig. 2). Likewise $(1-G)$ represents the As contribution from $\phi = -\frac{1}{8} \Delta$. The (111) Fourier coefficient for this distribution

function $g(\phi)$ is:

$$F_1 = Ge^{2\pi i (\frac{1}{8} + \Delta)} + (1-G)e^{2\pi i (-\frac{1}{8} + \Delta)} \quad (17)$$

With $F_1 = |F_1|e^{2\pi i \phi}$, the amplitude of the Fourier coefficient, which is directly related to the coherent fraction f_c , is:

$$|F_1| = [2G^2 - 2G + 1]^{1/2} \quad (18)$$

and the phase of the Fourier coefficient, which is directly related to the coherent position ϕ_c , is:

$$\phi_1 = \frac{1}{2\pi} \tan^{-1} \left[\frac{2G-1+\tan(2\pi\Delta)}{(1-2G)\tan(2\pi\Delta)+1} \right] \quad (19)$$

The distribution function $g(\phi)$ in Eq. (16) assumes that the Ga and As atoms are fixed points relative to the diffraction planes. To include thermal vibrations, the delta functions of Eq. (16) are replaced with normalized Gaussian functions having widths $\sigma = \sqrt{\langle u^2 \rangle}/d$, where $\sqrt{\langle u^2 \rangle}$ is the root mean square of the vibrational amplitude. We will use $\sqrt{\langle u^2 \rangle} = 0.107 \text{ \AA}$ for both Ga and As at room temperature. (Note that $e^{-2\pi^2 \sigma^2} = e^{-M} = .979$) The consideration of thermal vibrations adds a prefactor to Eq. (18) yielding:

$$|F_1| = e^{-M} [2G^2 - 2G + 1]^{1/2} \quad (20)$$

In examining the expressions given in Eqs. (19) and (20), it is evident that for an electron energy region with no contribution from As sites (i.e. $G=1$), $|F_1| = e^{-M} = .979$ and $\phi_1 = \frac{1}{8} + \Delta$.

The smallest Fourier amplitude is produced for an equal contribution from the Ga and As sites (i.e. $G=1/2$). In this case $|F_1| = e^{-M}/\sqrt{2} = 0.692$ and $\phi_1 = \Delta$. For the Ge(111) case, it is not possible to spectroscopically discriminate between the $\phi = \frac{1}{8}$ and $\phi = -\frac{1}{8}$ positions; therefore the coherent fraction and position for Ge(111) should ideally be $f_c = e^{-M}/\sqrt{2}$ and $\phi_c = 0$ for all electron energy regions.

The experimental electron yields versus angle for the electron energy regions designated in Fig. 5e, 5b and 5a are shown in Figs. 7, 8 and 9 respectively. The χ^2 fitted curves are based on Eq. (15). The χ^2 fit determined values for f_c and ϕ_c and the fixed z values are shown in Table 2 for the $E_Y = 15.1 \text{ keV}$ and 10.07 keV GaAs(111) data sets. As previously stated, the average electron escape depth values z were determined from the corresponding Ge(111) data sets.

The experimental reflection curve for each of these X-ray standing wave scans is also shown in Figs. 7, 8 and 9. The fitted theoretical reflectivity curves were used to determine the angular scale for each scan. The angular range from each of the three fits was $103 \pm 2 \text{ \mu rad}$.

The theoretical reflectivity and E-field intensities for the 15.1 keV scan were not convoluted with the angular output from the asymmetrically cut ($\psi = 7^\circ$) Si(111) monochromator crystal, since the ratio of this width (ω_{mc}) to the GaAs(111) acceptance width was $1/12$,

However, since this ratio was approximately $1/4$ for the x-ray standing wave scans at 10.372 keV and 10.07 keV , the theoretical

GaAs (111) reflectivity and intensity curves were convoluted by the angular output from the monochromator.

Since the experimental angular scan range for each of the separate X-ray energies was maintained at a constant setting ($\pm 1\%$), it was possible to confirm the f' values in Table 1 to within 10% by noting that the theoretically fit determined range of 103 ± 2 μ rad was maintained for each of the five energies and by assuming the values at 15.1 keV. If wanted, this precision can easily be increased.

IV. Discussion

From the average electron escape depth values listed in Table 2 it can be seen that as the electron energy loss for a particular electron emission process increases, the depth z , as should be expected, also increases. Furthermore, these depth values fall in line with empirically calculated values⁷ for the emergence length of electrons emitted in Ge; $L_e = 250 E_i^{1.4}$ (\AA), where E_i is the initial kinetic energy of the escaping electron in keV. For Ge L photoelectrons ejected by photons having energy $E_Y = 10$ keV, $L_e = 5200$ \AA . This $E_i^{1.4}$ dependence was used for scaling down the measured z values of the Ge(111) data taken at $E_Y = 10.9$ keV to the values listed in Table 2 for $E_Y = 10.07$ keV. For a more accurate description of the electron escape depth distribution the delta function approach could be replaced by a description similar to that being used in recent DCEMS (depth selective conversion electron M6ssbauer spectroscopy) investigations²⁸.

Due to the low energy resolution of the electron counter, it was not possible to spectroscopically separate the electrons emitted from the Ga atomic site from those emitted from the As atomic site. Therefore the measured coherent position values ϕ_c in Table 2 do not reach the pure Ga value of $0.125 + \Delta$ or the pure As value of $-0.125 + \Delta$. The data taken just above the Ga K absorption edge (Figs. 5b and 8) most closely approaches this one site conditions since the Ga KLL Auger electron yield is anomalously very high at this energy. The measured coherent position for electron energy region A of Fig. 5b was $\phi_c = 0.093 \pm .004$. However, when in the vicinity of the absorption edge, it is necessary to take into account the slightly dispersive arrangement between the Si(111) monochromator and GaAs(111) sample crystal, since the energy dependence of the dynamical diffraction process at the absorption edge is significant over the energy window of the monochromator.

The most straightforward way of testing this data analysis for an X-ray energy dependent diffraction plane shift is to look for a shift in the measured coherent position ϕ_c for electron energy regions that have the same distribution of inelastic scattering sources at two different X-ray energies.

For this comparison we will choose the highest electron energy region in the $E_Y = 15.1$ keV scan and any of the electron energy regions in the $E_Y = 10.07$ keV scan. These regions have comparable Ga contributions G , since each has no K-photoelectrons nor any K-Auger electrons, and since the total non-K photoelectric cross sections per atom (Ref. 27) for Ga to As atoms have the same ratios at 15 keV and 10 keV. Based on these non-K photoelectric cross sections the Ga contribution in all four of these electron energy regions should be $G = 0.43$. From Eq. (19) it can be seen, that for constant G , a shift in the coherent position ϕ_c is directly attributable to a shift in the diffraction plane position Δ_{111} . Since the coherent position for the three regions of the $E_Y = 10.07$ keV scan is $\phi_c = -0.010 \pm .006$ and since $\phi_c = 0.002 \pm .004$ for region E of the 15.1 keV scan, it can be seen that there is an energy dependent diffraction plane shift of $0.012 \pm .007$. From the atomic scattering factors given in Table 1 this shift was calculated as being 0.007. The difference between our measured fractional shift of .012 and the more accurate value of 0.007 corresponds to an absolute distance of 0.016 \AA . This gives an indication of the high precision of this measuring technique.

We have also included in Table 2 the result for the ideal coherent fraction $|F_1|$ which is calculated from Eqs. (19) and (20) by using the measured coherent position ϕ_c along with the Δ_{111} values listed in Table 1. The comparison ratio $f_c/|F_1|$ shows a deviation from unity which can be caused by three different effects. (i) Due to experimental angular averaging $f_c/|F_1|$ never reaches unity for any of the electron energy regions. (ii) The presence of disordered bulk or disordered surface layers can reduce the coherent fraction for electrons with

a specific energy loss. This is in detail demonstrated elsewhere²⁵, however, any disorder of the bulk will reduce the coherent fraction for each photon energy accordingly. Any disordered surface layer will degrade f_c continuously with decreasing electron energy loss. Both effects can be excluded with the present set of data as summed up in Table 2. (iii) The different spatial distributions of the K, L, M and N electrons will influence the coherent fractions of electrons emitted from different orbitals. This will be visible in sudden variations of f_c at certain electron energies. Although such changes clearly show up in Table 2, a detector with higher energy resolution and better signal to noise ratio is needed to separate out this effect distinctively.

V. Conclusion

We have demonstrated that X-ray standing wave modulated electron emission measurements, with a low resolution electron counter, can be used to obtain valuable information about a crystal structure, such as the polarity, the degree of perfection and the position of the constituent atoms. With the high intensity of synchrotron radiation, it is possible to study very small crystal areas and by making use of the depth dependent energy loss process for electron emission, depth selective structural information is also obtainable. The tunability of the photon energy, which is provided by a synchrotron source, can be successfully applied to measure electron yields and reflectivity curves far away and in the vicinity of absorption edges. Thus making it possible to determine the anomalous dispersion parameters f' and f'' , which describe the energy dependence of the X-ray

scattering process. By using the X-ray standing wave picture for describing the dynamical scattering process in a zinc blende single crystal, the energy dependence of the position of the noncentrosymmetric diffraction planes was also demonstrated. Since this measuring technique makes it possible to separate the X-ray scattering process into its various contributing channels, further explorations should be made in this direction with a medium or high energy resolution electron detector. Also, proper care should be taken in the data evaluation for the case of strong inelastic scattering, by using a more generalized dynamical theory for X-ray scattering which would include the influence of the lattice structure on the fundamental scattering process²⁹.

Table 1

Calculation of GaAs(111) diffraction plane shift Δ_{111} from atomic scattering factors, (see Eq. (14)) using $f_{As}^0 = 28.170$ and $f_{Ga}^0 = 26.665$ from Ref. 18, f' and f'' values for 5 eV above the Ga (10.372 keV) and As (11.868 keV) K edges from Ref. 17, and the remaining f' and f'' values from Ref. 19 and 20. The absolute shift in \AA can be obtained by multiplying Δ_{111} by $d_{111} = 3.26 \text{ \AA}$.

Energy (keV)	f'_{Ga}	f'_{As}	f''_{Ga}	f''_{As}	Δ_{111}
15.1	-.15	-.64	2.10	2.59	0.003
11.868	-1.25	-8.0	3.31	5.8	-0.015
11.16	-1.93	-2.82	3.33	0.58	0.001
10.372	-6.0	-2.19	5.0	0.66	0.016
10.07	-3.55	-1.98	0.54	0.70	0.010

References

- 1) G. Borrmann, Z. Phys. A2, 157 (1941), and 127, 297 (1950).
- 2) B.W. Batterman, Phys. Rev. 133, A759 (1964).
- 3) S. Annaka, S. Kikuta, and K. Kohra, J. Phys. Soc. Jpn. 21, 1559 (1966).
- 4) A.M. Afanasev and S.L. Azizian, Acta Cryst. A37, 125 (1981).
- 5) J.A. Golovchenko, D.R. Kaplan, B. Kincaid, R. Levesque, A. Meixner, M.F. Robbins and T. Felsteiner, Phys. Rev. Lett. 46, 1454 (1981).
- 6) W. Schülke, Phys. Lett 83A, 451 (1981).
- 7) M.V. Kruglov, E.A. Sozontov, V.N. Shchemelev and B.G. Zakharov, Sov. Phys. Crystallogr. 22, 397 (1977) and references therein.
- 8) T. Takahashi and S. Kikuta, J. Phys. Soc. of Jpn. 47, 620 (1979).
- 9) J.A. Golovchenko, B.W. Batterman and W.L. Brown, Phys. Rev. B 10, 4239 (1974).
- 10) P.L. Cowan, J.A. Golovchenko, and M.F. Robbins, Phys. Rev. Lett. 44, 1680 (1980).
- 11) J.A. Golovchenko, J.R. Patel, D.R. Kaplan, P.L. Cowan and M.J. Bedzyk, Phys. Rev. Lett. 49, 560 (1982).
- 12) V.G. Kohn, M.V. Kovalchuk, R.M. Imamov, B.G. Zakharov, and E.F. Lobanovich, Phys. Stat. Sol. A71, 603 (1982).
- 13) P. Trucano, Phys. Rev. B13, 2524 (1976).
- 14) J.R. Patel and J.A. Golovchenko, Phys. Rev. Lett. 50, 1858 (1983).
- 15) B.W. Batterman and H. Cole, Rev. Mod. Phys. 36, 681 (1964).
- 16) Z.G. Pinsker, "Dynamical Scattering of X-Rays in Crystals", Springer Verlag (1978).
- 17) T. Fukamachi, S. Hosoya, T. Kawamura, and M. Okunuki, Acta Cryst. A35, 828 (1979).
- 18) J.H. Hubbell and I. Øverbø, J. Phys. Chem. Ref. Data 8, 69 (1979).
- 19) "International Tables for X-Ray Crystallography", Vol. III, Kynoch, Birmingham, England (1974).
- 20) L. Gerward, Nucl. Instr. Meth. 181, 11 (1981).
- 21) G. Materlik and J. Zegenhagen, to be published.
- 22) N. Hertel, M.V. Kovalchuk, A.M. Afanesev and R.M. Imanov, Phys. Lett. 75A, 501 (1980).

Table 2

Data Analysis (see Figs. 5a, 5e, 7 and 9)
 * Ge(111) data at $E_{\gamma} = 10.9$ keV.

E_{γ} (keV)	Electron Energy Region	Average Electron Escape Depth z(\AA)	Coherent Fraction $f_c(+.01)$	Coherent Position $\phi_c(+.004)$	Ideal Coherent $ F_c $	CaAs(111) $\frac{f_c}{ F_c }$	Ge(111) $\frac{f_c}{ F_c }$
15.1	A	920	0.69	-0.022	0.70	0.92	0.97
15.1	B	1060	0.64	+0.036	0.71	0.90	0.95
15.1	C	1430	0.67	-0.035	0.71	0.94	0.97
15.1	D	1150	0.67	-0.040	0.72	0.94	0.97
15.1	E	880	0.63	+0.002	0.69	0.91	0.95
10.07	A	1170	0.70	-0.012	0.70	0.99	0.95*
10.07	B	700	0.68	-0.010	0.70	0.97	0.94*
10.07	C	650	0.55	-0.008	0.70	0.79	0.87*

- 23) N. Hertel, thesis, University of Aarhus, (1981).
- 24) A. Krolzig, G. Materlik and J. Zegenhagen, Nucl. Instr. Meth. 208, 613 (1983).
- 25) M. Bedzyk, G. Materlik and M.V. Kovalchuk, to be published.
- 26) K. Siegbahn et al., "ESCA", Nova Acta Regiae Societatis Scientiarum Upsaliensis Ser. IV, Vol. 20, Almqvist, Wiksells Boktryckeri ab, Uppsala (1967).
- 27) G. Hildebrand, J.D. Stephenson and H. Wagenfeld, Z. Naturforsch. 30A, 697 (1975).
- 28) G.N. Belozerskii, C. Bohm, T. Ekdahl and D. Liljequist, Nucl. Instr. and Meth. 192, 539 (1982).
- 29) G. Molière, Ann. de Phys. 35, 272 (1939) and ibid. 297.

- Fig. 1 GaAs(111) theoretical reflection curves at —: $E_Y = 10.07$ keV, ---: $E_Y = 10.372$ keV, —·—: $E_Y = 11.16$ keV, — — —: $E_Y = 11.868$ keV and -·-·-: $E_Y = 15.1$ keV for the σ polarization state.
- Fig. 2 Schematic view showing the position of the noncentrosymmetric GaAs(111) diffraction planes (dashed lines) relative to the Ga atoms (open circles) and As atoms (closed circles). Parameter Φ locates positions in this structure in the (111) direction relative to a (111) diffraction plane, which is shifted by an amount Δ relative to a centrosymmetric (111) diffraction plane.
- Fig. 3 The angular variation of the GaAs(111) reflectivities (R) and E-field intensities (I_{Ga} and I_{As}) at the Ga and As atomic sites for —: $E_Y = 10.372$ keV (5 eV above the Ga K-edge) and ---: $E_Y = 11.868$ keV (5 eV above the As K-edge) (for the σ polarization state).
- Fig. 4 Experimental set-up (schematic side view).
- Fig. 5 Off Bragg GaAs electron yield spectra collected with a gasflow proportional detector at incident X-ray energies in the vicinity of the respective K-absorption edges of Ga and As. Due to the E_Y dependent stopping power of the I_0 ionization chamber, the partial yield curves a-e were multiplied by 0.86, 0.91, 1.0, 1.1 and 2.0, respectively. The absorption spectrum that was obtained while calibrating the incident X-ray energy scale for this set of experiments is shown

as a side view on the left. RP: Reference Pulser.

Fig. 6 Electron yield spectra collected at different angular positions of the rocking curve, while Bragg diffracting from a GaAs(111) single crystal with a 15.1 keV incident X-ray beam. The corresponding rocking curve, shown in Fig. 7, illustrates the angular scale.

Fig. 7 Reflection data and theory for Bragg diffraction from the GaAs(111) sample at $E_{\gamma} = 15.1$ keV and the corresponding angular variation to the electron yields of electron energy regions A, B, C, D, E (see Fig. 5e). The electron yield scale corresponds to the bottom curve. Subsequent curves are given a 0.5, 1.0, 1.5 etc. offsets, respectively.

Fig. 8 Same as fig. 7, but for $E_{\gamma} = 10.372$ keV (see fig. 5b).

Fig. 9 Same as fig. 7, but for $E_{\gamma} = 10.07$ keV (see fig. 5a).

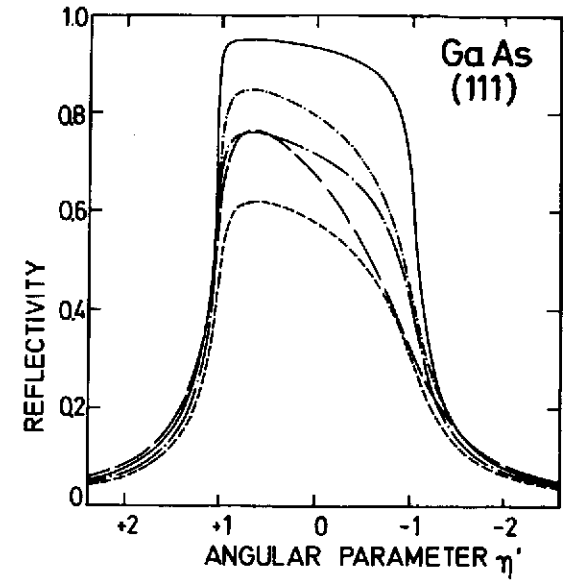
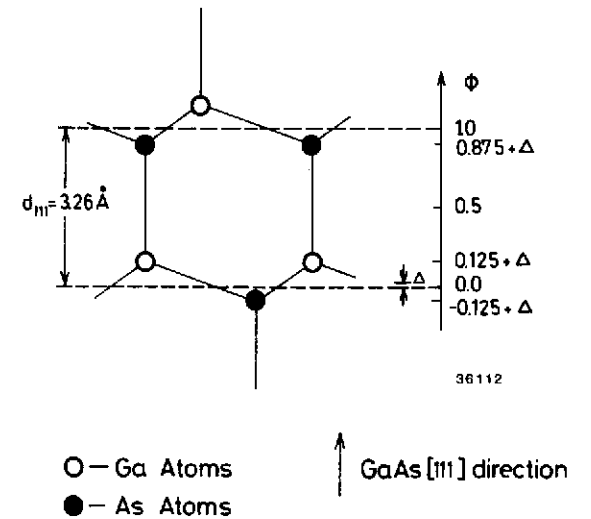


Fig. 1

36103



36112

Fig. 2

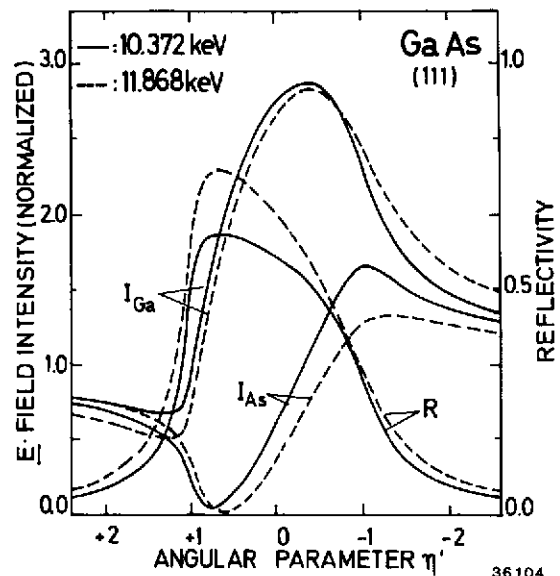


Fig. 3

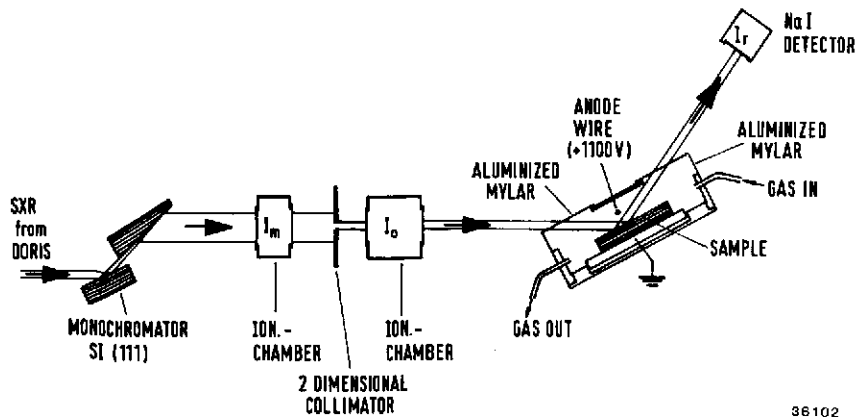


Fig. 4

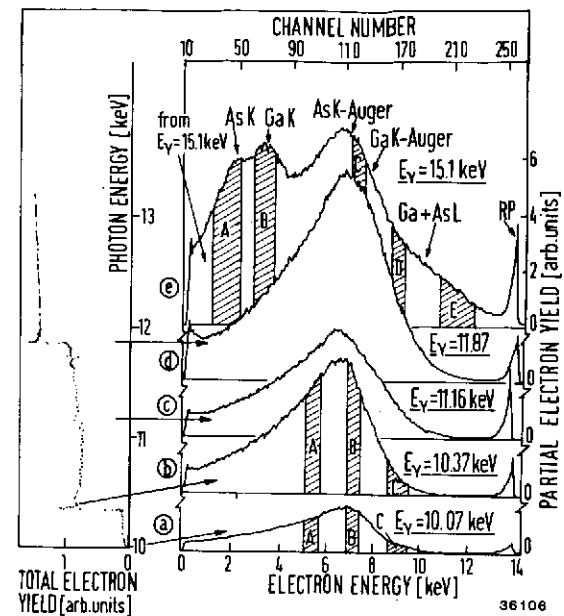


Fig. 5

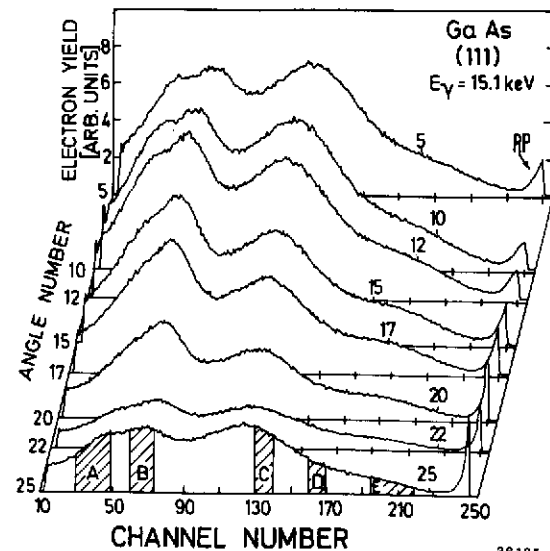


Fig. 6

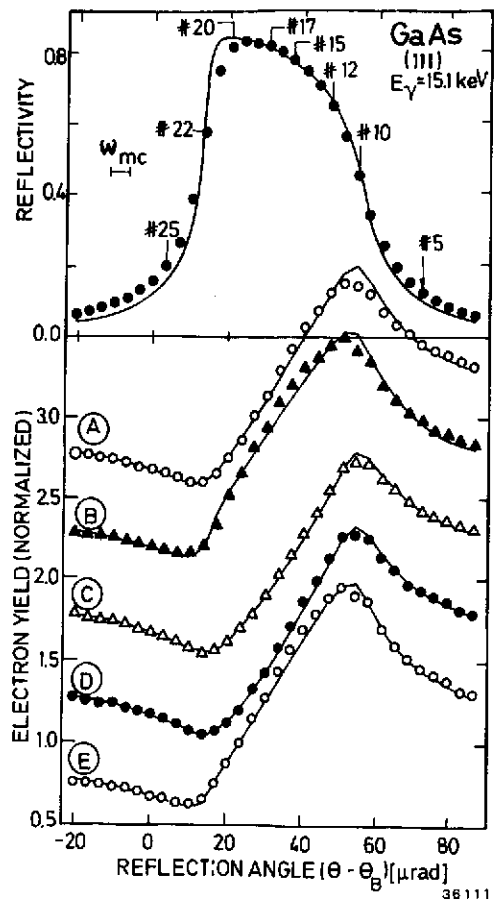


Fig. 7

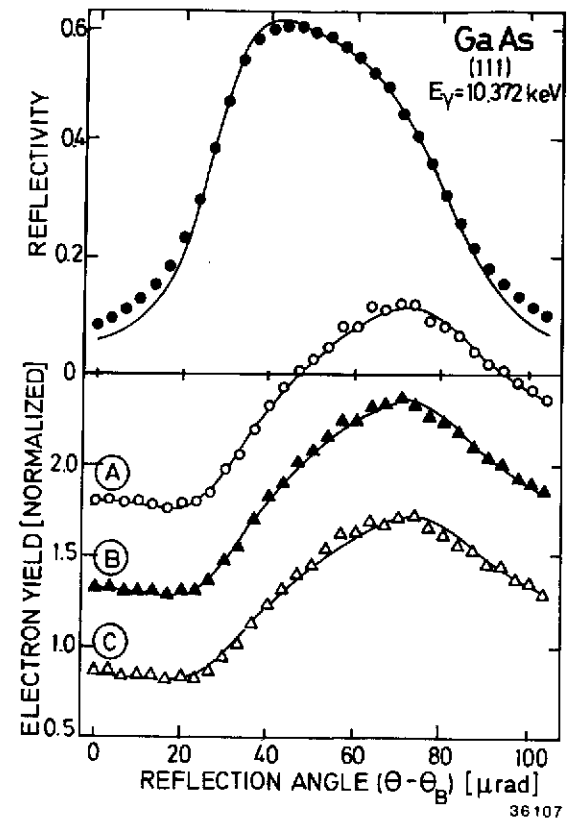
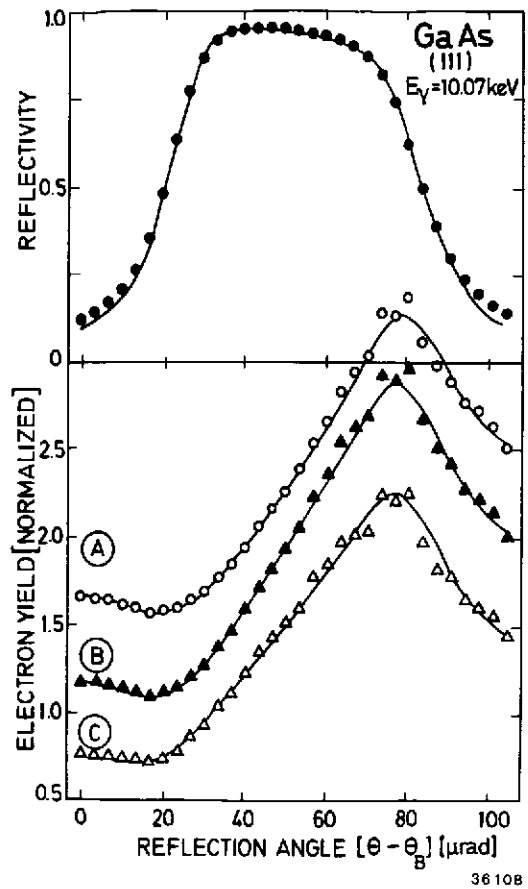


Fig. 8



3610B

Fig. 9

